Depletion forces between nonspherical objects

P.-M. König,[1,2] R. Roth,[1,2] and S. Dietrich[1,2]

[1]*Max-Planck-Institut für Metallforschung, Heisenbergstrasse 3, D-70569 Stuttgart, Germany*

[2]*Institut für Theoretische und Angewandte Physik, Universität Stuttgart, Pfaffenwaldring 57, D-70569 Stuttgart, Germany*

We extend the insertion approach for calculating depletion potentials to the case of nonspherical solutes. We suggest to employ the recently developed curvature expansion of density profiles close to complexly shaped walls. The approximations introduced in the calculation by the use of the curvature expansion and of weight functions for nonspherical objects can be tested independently. As an application for our approach we calculate and discuss the depletion potential between two hard oblate ellipsoids in a solvent of hard spheres. For this system we calculate the entropic force and torque acting on the objects.

PACS number(s): 82.70.Dd, 61.20.Gy

I. INTRODUCTION

If macromolecules such as colloids are immersed in a solvent of smaller particles, the difference in size makes it useful to describe this mixture in terms of effective interactions by integrating out the degrees of freedom of the solvent. The resulting interactions between particles of the remaining larger component are often referred to as depletion interactions. Such depletion forces have been studied in detail both theoretically [1–6] and experimentally [7–9]. Most theoretical approaches are based on a brute-force approach in which the solutes are frozen in a given configuration and thereby turned into an external field for the solvent [3,4,10]. From the inhomogeneous structure of the solvent in the external field due to two fixed solute particles one can calculate the solvent mediated effective force acting on the solutes. This brute-force approach turns out to be very time consuming because for each separation and orientation, for which one wants to determine the depletion force, the inhomogeneous solvent distribution has to be calculated anew.

The insertion approach to depletion potentials [6] differs in character in that there only one solute particle is fixed. The advantage is that the calculation of the solvent density profile in the external field of a single solute is usually much simpler and hence computationally less demanding. The potential of the depletion force can be determined from the solvent density profile close to one solute by inserting the second solute into the system using the potential distribution theorem [11]. However, for the insertion step a theoretical description of a mixture consisting of solute and solvent particles is required. The insertion approach is usually implemented within density functional theory (DFT). If one of the solutes is spherical by using integral-equation theory it is also possible to calculate depletion potentials in a single step from the knowledge of the density distribution of the solvent [12,13].

So far, most studies of depletion forces have been focused on rather simple geometries, such as the force between a big sphere and a planar wall or between two big spheres in a solvent of small spheres. For these symmetric systems the depletion potential depends on the sphere-wall or the sphere-sphere separation as the only parameter characterizing the configuration. In addition, for these geometries the use of the aforementioned insertion approach is facilitated by the avail-

ability of reliable density functional theories for hardsphere mixtures.

In colloidal mixtures one often encounters more complex particle shapes both of the solute and solvent particles. However, the understanding of depletion potentials for nonspherical objects is still rudimentary. The corresponding calculations are much more challenging because in these cases the depletion potential depends not only on the separation between the solutes but also on their relative orientation. Based on depletion potentials, it is possible to study the complex phase behavior of colloidal mixtures within an effective one-component Hamiltonian. Furthermore, our approach should prove useful for the study of effective interactions between a complexly shaped macromolecule and a cavity, which serves as a biologically inspired model system of a key and lock system [12].

A first extension beyond the mixture of spheres is the case of spherical solutes immersed in a solvent of nonspherical particles. Depletion agents such as thin rods [14–17] or infinitely thin platelets [18–20] can generate big depletion effects even at rather low solvent concentrations [9]. The depletion potential in these cases can be calculated in the limit of small solvent densities so that correlations among the depletion agents are small. Similar in spirit is also the calculation of the depletion force between spheres in a solvent of a liquidcrystal in its nematic phase [21,22], for which the strong correlations between particles of the liquid crystal are taken into account effectively by reducing their orientational degrees of freedom. The strength of the depletion interaction is then estimated by excluded volume calculations, following the ideas of Asakura and Oosawa [1,2].

A second, more complicated situation is the one studied in Ref. [23], where one spherocylinder immersed in a spherical solvent close to a planar wall was considered. These calculations employed the insertion approach. The resulting depletion potential depends not only on the separation of the solute from the wall but also on its orientation. Hence in addition to the depletion force an entropic torque acts on the solute.

There are recent studies of depletion forces between two spherocylinders in a solvent of spheres which overcome the Asakura-Oosawa approximation [1,2]. Using a three-dimensional integral-equation theory, Kinoshita [10,13] showed that the corresponding depletion potential displays a

rich behavior and depends sensitively on the path along which the spherocylinders approach each other. Similar findings were reported in a simulation study, in which the depletion potential was determined by the acceptance ratio method [24].

Here we extend the insertion approach to depletion potentials [6] to the case of nonspherical objects. In Sec. II we recall the basic theory and highlight how the geometry of the solutes can be accounted for. We test the elements of the theory in Sec. III. As an application we discuss the depletion potential between two ellipsoids in Sec. IV. We conclude in Sec. V.

II. THEORY

We follow the versatile and successful approach to calculating depletion potentials between two objects, a and b, immersed in a solvent within the framework of DFT [6], which is referred to as the insertion approach. To this end we fix one of the objects, say a, at the origin at a given orientation so that it acts as an external potential for the solvent particles. In response to this external potential, the solvent particles aquire an inhomogeneous equilibrium number density distribution $\rho_s(\mathbf{r})$. In the fluid phase, the case we are interested in here, $\rho_s(\mathbf{r})$ shares the spatial symmetry with that of object a. If object a is a sphere, the density distribution $\rho_s(\mathbf{r})$ also possesses spherical symmetry. In a second step we insert the second object, denoted by b, into the inhomogeneous solvent at position $\mathbf{r}$ and with relative orientation $\boldsymbol{\omega}$. As a result of this insertion the grand potential $\Omega(\mathbf{r}, \boldsymbol{\omega})$ of the system changes. The depletion potential is given by [6]

$$W(\mathbf{r}, \boldsymbol{\omega}) = \Omega(\mathbf{r}, \boldsymbol{\omega}) - \Omega(\mathbf{r} \rightarrow \infty, \boldsymbol{\omega}), \quad (1)$$

which can be rewritten in terms of the one-body direct correlation function $c_b^{(1)}(\mathbf{r}, \boldsymbol{\omega}) = -\beta \delta \mathcal{F}_{ex}/\delta \rho_b(\mathbf{r}, \boldsymbol{\omega})$ [6]:

$$\beta W(\mathbf{r}, \boldsymbol{\omega}) = c_b^{(1)}(\mathbf{r} \rightarrow \infty, \boldsymbol{\omega}) - c_b^{(1)}(\mathbf{r}, \boldsymbol{\omega}). \quad (2)$$

For the numerical calculation of $c_b^{(1)}(\mathbf{r}, \boldsymbol{\omega})$ two challenges have to be overcome: (i) the *accurate* calculation of the density profile $\rho_s(\mathbf{r})$ of solvent particles around an object of complex shape, and (ii) the insertion of a nonspherical object into an inhomogeneous solvent of spheres. Since both of these problems require nonstandard approaches, in the following we shall pay special attention to them.

Although our approach is flexible and can also treat soft solvent-solvent and solute-solvent interactions, in the following we shall restrict our considerations to the case of hardcore interactions. The solvent is represented by a hard-sphere fluid characterized by its radius R and bulk density ρ_s or bulk packing fraction $\eta_s = 4\pi R^3 \rho_s/3$. The solute-solvent interaction is infinitely repulsive in the case of overlap and zero otherwise.

A. Density profiles and weighted densities

1. Curvature expansion

Concerning the first issue of calculating the density profile around nonspherical objects we apply ideas of the recently suggested and successfully tested curvature expansion of the density profile [25]. The curvature expansion is expected to represent the density distribution around the nonspherical object more accurately than a corresponding three-dimensional calculation on a cubical grid. For the present problem, it turns out to be useful to take the intrinsic structure of fundamental-measure theory (FMT) functionals [26] into account and to extend the idea of the curvature expansion to other quantities like the free energy density and weighted densities (see Sec. II A 3).

We start by introducing normal coordinates. Any point $\mathbf{r}$ outside the fixed object a can be reached from $\mathbf{R}$ as the point closest to $\mathbf{r}$ on the parallel surface of the object, where the density profile $\rho_s(\mathbf{r})$ vanishes discontinuously. This particular surface is special to the case of hard-core solute-solvent interaction; however, it is possible to employ any parallel surface as long as all the calculations are in line with this definition of $\mathbf{R}$.

For the vector connecting the points $\mathbf{R}$ and $\mathbf{r}$ one has $\mathbf{R} - \mathbf{r} = u\mathbf{n}(\mathbf{R})$, where $\mathbf{n}(\mathbf{R})$ is the unit vector normal to the parallel surface at point $\mathbf{R}$ and u is the normal distance. At point $\mathbf{R}$ the parallel surface exhibits two principle radii of curvature R_1 and R_2 leading to the dimensionless mean and Gaussian curvatures $H(\mathbf{R}) = (R/R_1 + R/R_2)/2$ and $K(\mathbf{R}) = R^2/(R_1 R_2)$, respectively.

As an ansatz for the density profile we employ [25]

$$\rho_s(\mathbf{r}) = \rho_s^P(u) + H(\mathbf{R})\rho_s^H(u) + K(\mathbf{R})\rho_s^K(u) + H(\mathbf{R})^2\rho_s^{H2}(u)$$

$$+ H(\mathbf{R})^3\rho_s^{H3}(u) + H(\mathbf{R})K(\mathbf{R})\rho_s^{HK}(u) \cdots, \quad (3)$$

which factorizes the local geometry of object a at position $\mathbf{R}$, specified by the local mean and Gaussian curvature $H(\mathbf{R})$ and $K(\mathbf{R})$, respectively, and the structure of the solvent via the coefficient functions $\rho_s^\xi(u)$ with $\xi = P, H, K, \ldots$. This separation of geometry and the coefficient functions allows one to infer $\rho_s^\xi(u)$ from simple geometries with high symmetry, such as a fluid close to planar, spherical, or cylindrical walls. The functions $\rho_s^\xi(u)$ have been determined in Ref. [25]. There the direct comparison between a density profile predicted by the curvature expansion, based on these coefficient functions and obtained within DFT, with results from Monte Carlo simulations has demonstrated the high accuracy of this approach. Note that the curvature expansion of the density profile, Eq. (3), implicitly assumes that the curvature of the fixed object varies smoothly on its the surface. A sharp edge would be problematic because the mean curvature jumps from zero to a nonvanishing value at the edge.

2. Contact density on spherocylinders

On the surface of a spherocylinder both the mean and the Gaussian curvature vary discontinuously where the spherical cap meets the cylinder. Also this discontinuity of the curvatures cannot be captured fully by the curvature expansion.

In order to analyze the reliability of the curvature expansion we have performed a Monte Carlo simulation of a hardsphere fluid exposed to a spherocylinder. As parameters we have chosen $\eta_s = 0.3$ for the packing fraction of the fluid, $L = 10R$ for the length of the cylinder, and $R_{sc} = 4R$ for the
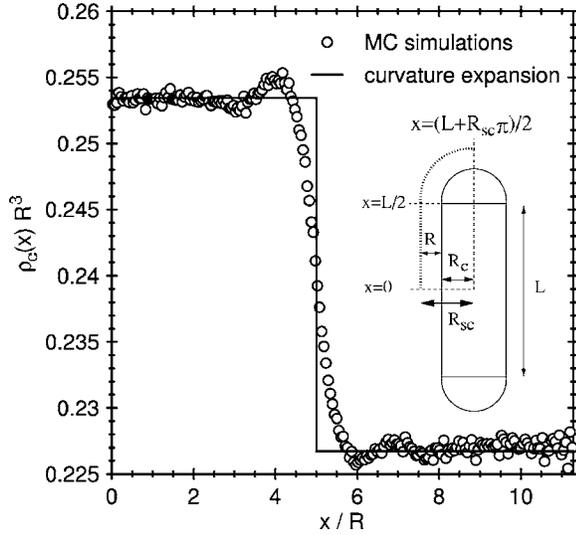
FIG. 1. The contact density $\rho_c(x)$ of a fluid of hard spheres with radius R and packing fraction $\eta_s=0.3$ at a hard spherocylinder with length $L=10R$ and radius $R_c=3R$ so that the contact density occurs at $R_{sc}=4R$. The path on the parallel surface of contact of the spherocylinder is parametrized by x, as is indicated by the dotted line in the inset. Note that the inset is not drawn to scale. According to the curvature expansion the contact value $\rho_c(x)$ jumps at $x=L/2$, where the cylindrical and the spherical parts meet, as shown by the full line. The symbols denote data from Monte Carlo simulations for $\eta_s=0.3$.

radius of the parallel surface at which the density profile discontinuously drops to zero. In this test we focus on the contact density $\rho_c(x)$ as the most sensitive quantity, where x parametrizes a path along the surface as depicted in the inset of Fig. 1. The density profile away from contact decays toward the bulk density and we verified that the effects of the discontinuity of the curvature decreases with increasing normal distance from the spherocylinder.

The dimensionless curvatures on the cylindrical part of the surface are $H=R/(2R_{sc})$ and $K=0$, while they are $H=R/R_{sc}$ and $K=(R/R_{sc})^2$ on the spherical caps. Accordingly, the curvature expansion predicts a jump in the contact value of the density profile where the spherical caps meet the cylinder. The result of the curvature expansion is plotted as the full line in Fig. 1. Note that in Eq. (3) only the three terms $\rho_s^P(u)$, $\rho_s^H(u)$, and $\rho_s^K(u)$ have a nonvanishing contact value and hence contribute to $\rho_c(x)$ [25,27].

In contrast to the jump of the contact density between constant values as predicted by the curvature expansion, in the computer simulations we find a smooth, slightly oscillatory transition between the contact densities at the cylindrical and the spherical part of the spherocylinder. In Fig. 1 the simulation data for $\rho_c(x)$ are shown as symbols. Interestingly, the spatial region of deviation between the simulation data and the prediction of the curvature expansion is relatively narrow.

3. Curvature expansion of the free energy density and of weighted densities

Although the density profile $\rho_s(\mathbf{r})$, as given by Eq. (3), is in principle sufficient for the calculations we intend to per-

form, it is numerically more efficient to exploit the particular form of fundamental-measure theory functionals [26] and extend the idea of the curvature expansion to weighted densities and the free energy density, i.e., to auxiliary functions of the FMT functional. Within FMT the one-body direct correlation function is given by

$$c_b^{(1)} = -\sum_\alpha \frac{\partial \Phi}{\partial n_\alpha} \otimes w_\alpha^b, \qquad (4)$$

where Φ is the excess free energy density and $\Psi_\alpha \equiv \partial\Phi/\partial n_\alpha$ depends on $\rho_s(\mathbf{r})$ in a complicated, nonlinear way. The convolution product is denoted as $\otimes$. Instead of calculating Ψ_α from $\rho_s(\mathbf{r})$ directly, we argue that $\Psi_\alpha(\mathbf{r})$ can be equivalently expanded in terms of powers of H and K and therefore can be written

$$\Psi_\alpha(\mathbf{r}) = \Psi_\alpha^P(u) + H(\mathbf{R})\Psi_\alpha^H(u) + K(\mathbf{R})\Psi_\alpha^K(u) + \cdots. \qquad (5)$$

One can adopt the point of view that curvature expansions such as those given in Eqs. (3) and (5) are merely approximations of the functions $\rho_s(\mathbf{r})$ or $\Psi(\mathbf{r})$ that take the shape of the external potential into account in an efficient way. Within this line of arguments there is nothing special about the density distribution or any other function entering the DFT. Even auxiliary functions such as the weighted densities $n_\alpha(\mathbf{r})$ and $\Psi_\alpha(\mathbf{r})$ have a curvature expansion ensuring that the output of the DFT calculation has the form of Eq. (3).

A more systematic, albeit more involved, point of view, which we present here only as a sketch, starts with an approach similar in spirit to the one that leads to Eq. (3) [25] as a suitable form for the density profile. Here, however, we analyze the weighted densities, defined as follows:

$$n_\alpha(\mathbf{r}) = \int d\mathbf{r}' \rho_s(\mathbf{r}')w_\alpha(\mathbf{r},\mathbf{r}'), \qquad (6)$$

close to planar, spherical, and cylindrical walls. Our results suggest that analogous to the density profile [Eq. (3)] the weighted densities can also be expanded in terms of powers of the curvatures H and K. As in Ref. [25] we can determine uniquely the coefficient functions n_α^ξ for $\xi = P,H,K,H^2,HK,H^3$ up to third order in the inverse of the radii of curvatures inferred from planar, spherical, and cylindrical geometries. In order to obtain higher order contributions one would have to consider more complex wall shapes. The numerical accuracy of weighted densities calculated at more complex walls is, however, unsatisfactory and practically prevents a reliable decomposition into coefficient functions. Since we are interested in calculating the depletion potential between two *big* nonspherical objects immersed in a solvent of *small* spheres, the coefficient functions which we have determined are sufficient. For our approach to be quantitatively reliable, curvatures of the surface of the nonspherical objects should always be sufficiently small.

We therefore use as an ansatz for the weighted densities, following Ref. [25],

$$n_\alpha(\mathbf{r}) = n_\alpha^P(u) + H(\mathbf{R})n_\alpha^H(u) + K(\mathbf{R})n_\alpha^K(u) + \cdots, \qquad (7)$$

which we can insert into the free-energy density Φ or its derivative with respect to n_α, i.e., Ψ_α. Both Φ and Ψ_α are

highly nonlinear functions of n_α. However, by Taylor expanding Φ or Ψ_α into powers of n_α and by rearranging terms one can see immediately that the curvature expansions of Ψ_α follow directly from Eq. (7).

B. Insertion of nonspherical objects

We now turn to the second part of the present problem, i.e., the calculation of the insertion free energy [Eq. (2)] of the nonspherical object b. Note that the change in the grand potential due to the insertion of object b into a *homogeneous* bulk fluid at $\mathbf{r} \to \infty$ can be described by using the morphometric approach [25,27]. In the bulk, the change in the grand potential of the system cannot depend on the orientation of the inserted object, which simplifies the problem somewhat. Furthermore, it was shown that the problems even simplify further due to the separation of the geometry and the shape independent thermodynamical coefficients. In the morphometric approach, the insertion free energy of object b in a bulk fluid can be written [25,27]

$$-\beta^{-1} c_b^{(1)}(\mathbf{r} \to \infty, \boldsymbol{\omega}) = pV_b + \sigma A_b + \kappa C_b + \bar{\kappa} X_b, \qquad (8)$$

where p, σ, κ, and $\bar{\kappa}$ are the pressure, the planar wall surface tension, and two bending rigidities, respectively, which depend on the state of the bulk fluid and the interaction between the fluid and object b. These coefficients can be obtained in simple geometries. The corresponding geometrical measures V_b, A_b, C_b, and X_b describing the shape of object b are the volume, the surface area, and the integrated (over the surface area) mean and Gaussian curvature, respectively.

In order to calculate the convolutions in Eq. (4) the weight functions w_α^b for a nonspherical object are required. For this problem we employ Rosenfeld's formulation of fundamental measure theory generalized to convex hard bodies [28,29]. There are four scalar weight functions:

$$w_3^b(\mathbf{r}) = \Theta(|\mathbf{r} - \mathbf{R}_b(\theta, \phi)|), \qquad (9)$$

which defines the volume V_b of object b,

$$w_2^b(\mathbf{r}) = \delta(\mathbf{r} - \mathbf{R}_b(\theta, \phi)), \qquad (10)$$

which defines the surface area A_b of b,

$$w_1^b(\mathbf{r}) = \frac{H(\mathbf{r})w_2^b}{4\pi}, \qquad (11)$$

which defines the integrated (over the surface) mean curvature C_b of b, and

$$w_0^b(\mathbf{r}) = \frac{K(\mathbf{r})w_2^b}{4\pi}, \qquad (12)$$

which defines the integrated (over the surface) Gaussian curvature or Euler characteristics X_b of object b. Besides the scalar weight functions, which represent the geometrical properties of b, there are two additional vectorlike weight functions which are required for the deconvolution of the Mayer f function describing the interaction between nonspherical particles. The vectorlike weight functions are given by

$$\mathbf{w}_2(\mathbf{r}) = -\boldsymbol{\nabla} w_3^b(\mathbf{r}) = \mathbf{n}_b(\mathbf{r})\delta(\mathbf{r} - \mathbf{R}_b(\theta, \phi)), \qquad (13)$$

where $\mathbf{n}_b(\mathbf{r})$ is the unit vector of the surface normal at point $\mathbf{r}$, and

$$\mathbf{w}_1(\mathbf{r}) = \frac{H(\mathbf{r})\mathbf{w}_2(\mathbf{r})}{4\pi}. \qquad (14)$$

In a bulk system the vectorlike weighted densities $\mathbf{n}_2(\mathbf{r})$ and $\mathbf{n}_1(\mathbf{r})$ vanish. These weight functions have been employed successfully in the calculation of the depletion potential between a hard spherocylinder and a planar hard wall [23].

With Eqs. (2) and (4) we can now calculate the depletion potential $W(\mathbf{r}, \boldsymbol{\omega})$.

C. Force and torque

From the knowledge of the depletion potential $W(\mathbf{r}, \boldsymbol{\omega})$ it is possible to determine the entropic force and the entropic torque [23] acting on object b with orientation $\boldsymbol{\omega}$ at a given position $\mathbf{r}$. If object b is translated by an infinitesimal vector $\delta\mathbf{r}$, while keeping its orientation fixed, the depletion potential changes by $\delta W = -\mathbf{F} \cdot \delta\mathbf{r}$, which defines the depletion force

$$\mathbf{F}(\mathbf{r}, \boldsymbol{\omega}) = -\frac{\partial}{\partial\mathbf{r}} W(\mathbf{r}, \boldsymbol{\omega}). \qquad (15)$$

The torque acting on the object b can be calculated by a similar consideration, rotating object b by an infinitesimal angle $\delta\boldsymbol{\omega}$. The direction of $\delta\boldsymbol{\omega}$ is parallel to the axis of rotation and its modulus specifies the angle of rotation. If one keeps the center of b fixed at $\mathbf{r}$ and performs a rotation by $\delta\boldsymbol{\omega}$, the depletion potential changes by δW, so that $\delta W = -\mathbf{M} \cdot \delta\boldsymbol{\omega}$. Therefore we can write the entropic torque as [23] follows:

$$\mathbf{M}(\mathbf{r}, \boldsymbol{\omega}) = -\frac{\partial}{\partial\boldsymbol{\omega}} W(\mathbf{r}, \boldsymbol{\omega}). \qquad (16)$$

III. TEST: DEPLETION POTENTIALS BETWEEN ELLIPSOIDS AND SPHERES

Before we apply the above formalism to the calculation of the depletion potential between two nonspherical objects, we perform a test that enables us to estimate the errors introduced into the numerical calculation through the approximations we have made. One source of error is the use of the curvature expansion of the density profile $\rho_s(\mathbf{r})$ [Eq. (3)] and of the derivatives $\Psi_\alpha(\mathbf{r})$ of the excess free-energy density [Eq. (5)]. It introduces an approximation because we have to truncate the expansion after the third order in the inverse radii of curvature. Another source of error is the application of the FMT weight functions for nonspherical objects, which introduces a different approximation. The fact that these two approximations are very distinct in nature allows us to perform a stringent numerical test.

To this end we calculate the depletion potential between one big sphere and one big ellipsoid in a solvent of small spheres. In an *exact* treatment the depletion potential between these two objects would depend only on their relative
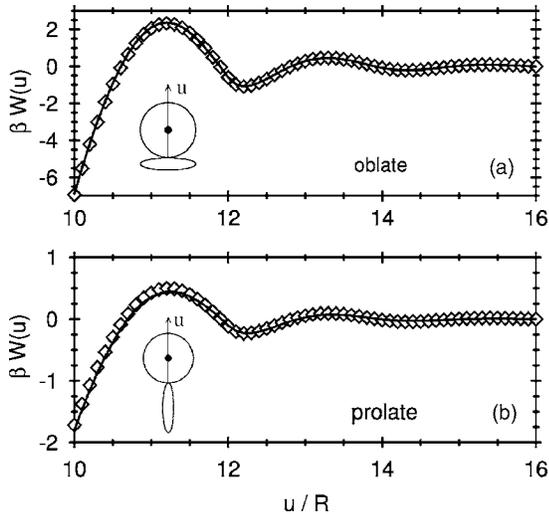
FIG. 2. Depletion interaction between an oblate (a) [prolate (b)] ellipsoid with half-axes $(10,10,4)R$ $[(4,4,10)R]$ and a sphere with $R_a=10R$. The center of the inserted sphere approaches the north pole of the fixed ellipsoid normal to the surface. Both particles touch if $u=R_a$. The symbols denote results obtained by approach (i), for which we employ FMT for convex objects, and the lines denote corresponding results from approach (ii), for which we use the curvature expansion. As both approaches involve approximations of very different nature, the excellent agreement is very likely to be due to the fact that the systematic error is very small in both approaches. We verified this observation also for ellipsoids with different half axes. For these data the depletion agent is a fluid of hard spheres with radius R modeled via the White Bear version of FMT. The bulk packing fraction is $\eta_s=0.3$. Note that the insets here and in the following figures are not drawn to scale.

position and orientation. In the numerical implementation of the insertion method we can follow two different routes which make independent use of the different approximations. We can choose to fix either the sphere and insert the ellipsoid or fix the ellipsoid and insert the sphere. By the choice of the particle fixed at the origin we decide about the symmetry of the external potential and how to calculate the density distribution of the solvent.

If we choose to fix the big sphere the calculation of the density profile $\rho_s(\mathbf{r})=\rho_s(r)$ is straightforward and, using the spherical symmetry of the problem, it was established that the results agree extremely well with, e.g., Monte Carlo simulations. Along this route, the main approximation for the calculation of $W(\mathbf{r},\boldsymbol{\omega})$ stems from using the weight functions for the ellipsoid.

Note that the resulting depletion potential $W(r,\boldsymbol{\omega})$ depends on both the orientation $\boldsymbol{\omega}$ of the ellipsoid relative to the vector $\mathbf{r}$ connecting the centers of the ellipsoid and the sphere and the distance r between the ellipsoid and the sphere. For this test, however, we fix the orientation and consider the approach between the ellipsoid and the sphere along the surface normal of the sphere for the chosen orientation of the ellipsoid. In Fig. 2 we show the depletion potential between a big sphere, denoted as object a, with radius $R_a=10R$ and an oblate ellipsoid with half axes $(10,10,4)R$ (a), and between a sphere with radius $R_a=10R$ and a prolate

ellipsoid with half axes $(4,4,10)R$ (b). In both cases the solvent is a fluid of small spheres with a packing fraction $\eta_s=0.3$, which we model by the White Bear version of FMT [30,31]. The insets in Fig. 2 depict the orientation between the ellipsoids and the sphere chosen in the calculation. The symbols denote the results obtained via the first route, corresponding to a fixed sphere.

Along the second route, we fix the ellipsoid at the origin so that it acts as an external potential for the solvent spheres. Now we employ the curvature expansion [Eq. (5)] in order to evaluate the derivatives of the excess free energy density $\Psi_\alpha(\mathbf{r})$. The weight functions we need in order to describe the insertion of the big sphere in Eq. (4) are well tested and are known to be accurate [6]. The results for the depletion potentials along the same paths between the sphere and the oblate and prolate ellipsoid obtained from this route are shown in Fig. 2 as lines.

We find that the results obtained from both routes agree extremely well, which provides confidence in the reliability of the approximations and the numerical approach. Only in the case of the prolate ellipsoid, for which the curvatures are considerably higher than in the case of the oblate ellipsoid, we find some deviations between the two routes close to the first potential barrier. However, these deviations are very small.

Close to contact between the sphere and the ellipsoids, one can employ arguments based on considerations about the overlap of excluded volumes [1,2,5]. In the case of high curvature one expects that the contact value of the depletion potential is considerably reduced compared to cases of low curvature. This expectation is confirmed by our results. In addition to the contact value, we find that the amplitude of the oscillations of the depletion potential for the oblate ellipsoid [Fig. 2(a)] is larger than the one for the prolate ellipsoid [Fig. 2(b)].

We conclude from the results of this test that both the curvature expansion of the functions $\Psi_\alpha(\mathbf{r})$ and the insertion of a nonspherical particle into an inhomogeneous solvent of small spheres work reliably.

IV. APPLICATION: DEPLETION POTENTIALS BETWEEN TWO ELLIPSOIDS

We can now turn to the calculation of the depletion potential between *two* nonspherical, convex objects. In order to accomplish this we have to combine both steps mentioned and tested above. First we fix one of the two nonspherical objects and thus turn it into an external potential for the solvent of small spheres. The structure of the resulting inhomogeneous solvent density distribution at a given bulk density is captured by the curvature expansion given by Eq. (5). In the second step we employ the insertion of a nonspherical object.

In order to illustrate our approach we calculate the depletion potential between two hard oblate ellipsoids with half-axes $(10,10,4)R$ in a solvent of hard spheres with radius R and bulk packing fraction $\eta_s=0.3$. The resulting depletion potential depends on both the relative orientation $\boldsymbol{\omega}$ of the two ellipsoids and the vector $\mathbf{r}$ connecting their centers and
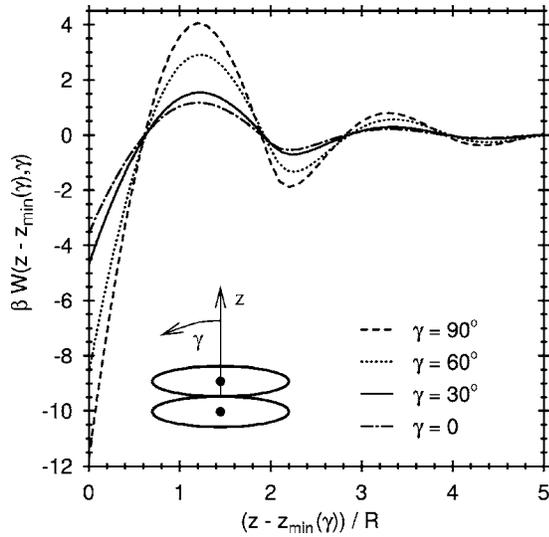
FIG. 3. Depletion interaction between two oblate ellipsoids with half-axes $(10, 10, 4)R$. The inserted particle approaches the north pole of the first ellipsoid perpendicular to its surface. γ denotes the angle between the z axis and the large half axis of the inserted ellipsoid (see the inset). If both ellipsoids are aligned (as drawn in the inset), i.e., $\gamma = 90°$, the minimal separation of the centers is $z_{min} = 8R$, while for $\gamma = 0$ it is $z_{min} = 14R$; $z_{min}(\gamma = 60°) \approx 9.53R$ and $z_{min}(\gamma = 30°) \approx 12.57R$. The positions of the extrema and the zeros are basically independent of γ. The solvent is a fluid of hard spheres with radius R and bulk packing fraction $\eta_s = 0.3$ and is modeled via the White Bear density functional.

thus depends on six variables. Out of this high-dimensional parameter space we select a few examples of paths along which we study the behavior of the depletion potential.

In the first example, the center of the inserted ellipsoid approaches the north pole of the fixed particle along the surface normal, as shown in the inset of Fig. 3. For this path we vary also the relative orientation $\boldsymbol{\omega}$ between the particles. Due to the symmetry of this configuration the orientation between the oblate ellipsoids can be expressed in terms of a single angle, which we denote by γ. If we choose $\gamma = 90°$, the ellipsoids are parallel and the minimal separation of their centers is $z_{min} = 8R$. At contact the overlap of excluded volume is larger than for any other value of γ. Hence the contact value of the depletion potential is most negative. For our choice of parameters we find $\beta W(z_{min}, \gamma = 90°) \simeq -12$ (see Fig. 3). In addition to the strong attraction close to contact, the depletion potential displays a pronounced oscillatory structure away from the contact.

This oscillatory structure of the depletion potential reflects mainly the properties of the solvent. The structure of the hard-sphere solvent normal to the surface displays oscillatory, exponentially decaying packing effects. We have shown previously [6] that beyond the first maximum the depletion potential between two spheres or between a sphere and a planar wall decays in a closely related, exponentially damped oscillatory fashion. The decay length and the wavelength of the oscillations in the depletion potential are exactly the same as those in the decay of the bulk pair correlation function. Only the amplitude of this decay and the phase of the oscillations depend on the shape and the orientation of the two solutes.
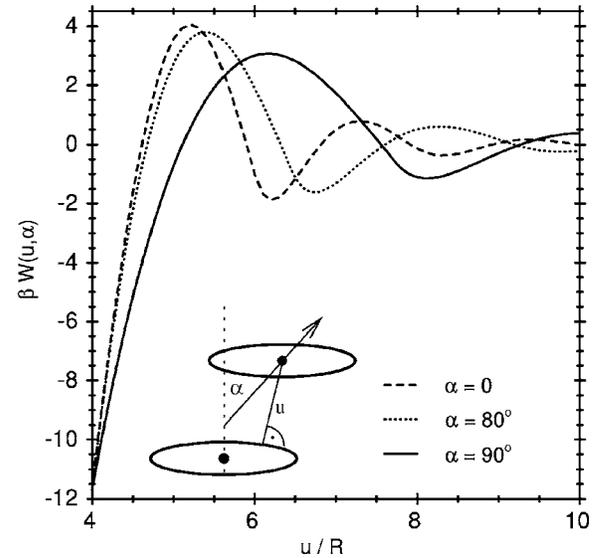
FIG. 4. Depletion potential for the same setup as in Fig. 3 with fixed $\gamma = 90°$. The angle α characterizes the straight line along which the center of the inserted ellipsoid is moved away from its contact position at the north poles (see the inset). The abscissa measures the normal (i.e., minimal) distance u of the center of the inserted ellipsoid from the surface of the fixed one. For small α the depletion potentials almost coincide due to the oblate shape $(10, 10, 4)R$ of the fixed ellipsoid.

As we decrease the value of γ from $90°$ to 0, thereby changing the relative orientation from parallel to normal, we find that the contact value as well as the potential barrier at $z - z_{min} \gtrsim R$ and the amplitude of the oscillations decrease monotonically; the positions of the extrema and of the zeros basically do not vary with γ.

In the second example the ellipsoids always approach each others north pole in a parallel configuration. The corresponding path of the centers is a straight line forming an angle α with the fixed direction of the small axes (see the inset of Fig. 4). In Fig. 4, by construction the path for $\alpha = 0$ is identical to the path with $\gamma = 90°$ in Fig. 3. Upon increasing α, at first the resulting depletion potential changes only slightly but for angles $\alpha \gtrsim 80°$ it is possible to observe a clear decrease in the wavelength of oscillation, which is most pronounced in the case of $\alpha = 90°$. This, however, is not a contradiction to the aforementioned universality of the oscillatory decay of the depletion potential, because this path cuts through the three-dimensional oscillatory structure of the solvent, which is organized *normal* to the surface of the fixed solute, at the angle α.

As pointed out earlier, for nonspherical objects it is also possible to keep the distance between their centers constant and change the relative orientation. From the corresponding change in the depletion potential we can obtain the entropic torque [23] acting on the inserted particle. For the same geometrical setup as in Fig. 3 we calculate the torque M for center to center separations $\Delta z / R = 10, 12, 14$, and 16. Due to the symmetry of this setup the entropic torque acting on the inserted ellipsoid, relative to its center, is parallel to the rotation $\boldsymbol{\omega}$, i.e., $\mathbf{M}(\Delta z, \gamma) = M(\Delta z, \gamma) \mathbf{n}_\gamma$, with $\mathbf{n}_\gamma = \boldsymbol{\omega} / \omega$ and
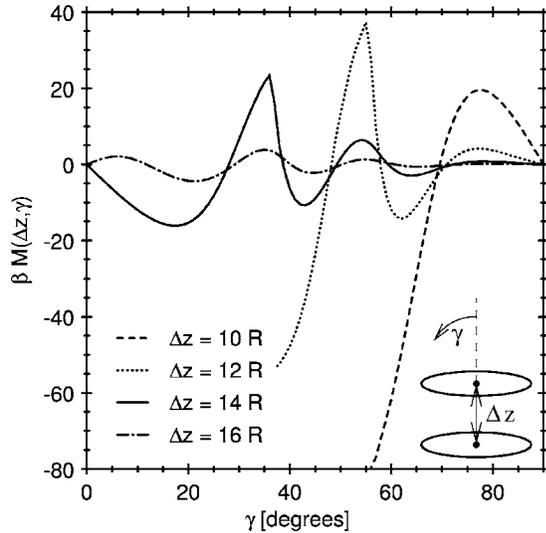
FIG. 5. Entropic torque between two oblate ellipsoids with half-axes $(10,10,4)R$ immersed in a solvent of hard spheres with radius R as sketched in the inset. The angle γ parametrizes the rotation of the inserted ellipsoid and Δz denotes the distance between the centers. The ellipsoids are aligned such that the vector connecting their centers runs through the north poles of the fixed (lower) ellipsoid. For this setup the entropic torque M is given by $M = -\partial W / \partial \gamma$ [23]. If $\Delta z > 8R$, the inserted (upper) ellipsoid can be rotated as indicated in the inset and experiences an entropic torque. Positive values of M mean that the ellipsoid is pushed toward larger values of γ. The curves end if the two ellipsoids overlap due to the geometrical constraint. Note that the visible discontinuities in the first derivative of the curves for $\Delta z = 12R$ and $\Delta z = 14R$ are not artifacts. They occur if both ellipsoids come so close that just a single small sphere with radius R fits in between their surfaces. For $\Delta z = 16R$ the distance between the ellipsoids is large enough so that this effect does not occur.

$$M(\Delta z, \gamma) = -\frac{\partial W(\Delta z, \gamma)}{\partial \gamma}. \qquad (17)$$

The symmetry of the problem leads to $M(\Delta z, \gamma) = 0$ for $\gamma = 0$ and $90°$. A positive value of the torque acts on the inserted ellipsoid as to increase the angle γ (rotating it toward an orientation parallel to the fixed ellipsoid), while a negative value of M leads to a decrease of γ (rotating it toward an orientation normal to the fixed ellipsoid). Some typical examples of the torque as a function of γ for various values of Δz are shown in Fig. 5. For small values of Δz the amplitude of the torque is largest; however, the hard-core interaction prohibits small values of γ due to geometrical constraints. For larger separations Δz between the ellipsoids, the accessible range of values of γ increases until finally the inserted ellipsoid can rotate freely without encountering the fixed ellipsoid. Due to the symmetry of the problem the torque vanishes for $\gamma = 90°$ as well as for $\gamma = 0$, provided this orientation is accessible.

If for any relative orientation of the ellipsoids the minimal distance between the surfaces equals the diameter $2R$ of a solvent spheres, the torque exhibits a cusp, as can be seen in the cases of $\Delta z > 10R$. For $\Delta z = 10R$ this orientation occurs at

$\gamma = 90°$. Accordingly, for sufficiently large Δz no such cusps occur.

All these feature of the torque (see Fig. 5) are similar to those of the entropic torque acting on a spherocylinder close to a planar wall [23].

From these results, one can speculate how two freely floating ellipsoids most likely would approach each other. Similar to the case of a spherocylinder close to a planar wall [23] we find that the ellipsoids prefer to be parallel once they touch each other. This configuration corresponds to $\gamma = 90°$ in Fig. 3. In order to be able to overcome potential barriers while approaching, it is easier for the ellipsoids to approach with a relative orientation different from the parallel configuration. By first seeking contact in regions of high curvature, and then by adapting the orientation such that regions of low curvature get in contact with each other, potential barriers, which have to be overcome, are significantly reduced and the minimum of the depletion potential can be reached. This interpretation agrees with observations reported in Refs. [10,13,24] where the depletion potential between two spherocylinder was studied.

V. SUMMARY AND CONCLUSIONS

We have extended the density functional theory approach for calculating depletion potentials [6] to effective interactions between generally shaped convex particles with surface curvatures which vary smoothly. As in the previously studied [6] geometrically simple case of two spherical particles, it is most efficient to carry out the calculation in two steps. In the first step we obtain the inhomogeneous structure of the solvent close to a fixed object. In the second step we insert the second solute into the solvent and calculate the change in the grand potential using the potential distribution theorem. Both steps constitute new challenges due to the nonspherical geometry of the solutes.

For the calculation of the inhomogeneous solvent density distribution, we have shown that the curvature expansion, which previously was applied to study the density profile of a fluid [25], can be extended within FMT to an equivalent curvature expansion of the derivatives Ψ_α of the free energy density [Eq. (5)]. If the mean and Gaussian curvatures of the surface of the solute vary smoothly across its surface, the curvature expansion provides an efficient tool. Discontinuities in the curvatures, such as those observed at sharp edges or close to the spherical caps of a spherocylinder, cannot be captured fully by the curvature expansion in its present form (see Fig. 1).

For the insertion of a second particle into the inhomogeneous solvent we employ an extension of fundamental measure theory to nonspherical particles [28,29], which was used in the study of a spherocylinder close to a planar wall [30]. Since the curvature expansion of the density profile or of the free energy density and the application of FMT to nonspherical objects introduce approximations, it is necessary to verify the accuracy of our approach. To this end we have studied the depletion potential between one ellipsoid and a big sphere immersed in a hard-sphere solvent. In this case we have been able to carry out the calculations in two different

ways, which employ the various approximations of our approach independently. We have found excellent agreement between the two routes (see Fig. 2) which provides confidence for the scheme used. Furthermore, we have studied the depletion potential between two equally sized oblate ellipsoids. For this case we have illustrated the potential of our approach. From the resulting depletion potential (see Figs. 3 and 4) one can calculate the entropic force acting on the centers of the solutes as well as the entropic torque (Fig. 5). This provides a picture for the likely pathway of how two freely floating ellipsoids approach each other under the action of entropic forces.

Besides the application to colloidal mixtures of non-spherical objects and spheres, this approach should prove useful to studying biological inspired model key and lock systems [12], for which depletion interactions between non-spherical objects and geometrically structured substrates are considered. The nonspherical objects and the substrates display a perfect geometrical match, similar to biological macromolecules (key) which can form chemical bonds with a cavity (lock) only if they are sufficiently close together. The issue is how the key can be guided into the lock using a robust, chemically unspecific mechanism. Our present analysis provides first steps toward addressing this issue.

[1] S. Asakura and F. Oosawa, J. Chem. Phys. **22**, 1255 (1954).

[2] S. Asakura and F. Oosawa, J. Polym. Sci. **33**, 183 (1958).

[3] T. Biben, P. Bladon, and D. Frenkel, J. Phys.: Condens. Matter **8**, 10799 (1996).

[4] R. Dickman, P. Attard, and V. Simonian, J. Chem. Phys. **107**, 205 (1997).

[5] R. Roth, B. Götzelmann, and S. Dietrich, Phys. Rev. Lett. **83**, 448 (1999).

[6] R. Roth, R. Evans, and S. Dietrich, Phys. Rev. E **62**, 5360 (2000).

[7] D. Rudhardt, C. Bechinger, and P. Leiderer, Phys. Rev. Lett. **81**, 1330 (1998).

[8] C. Bechinger, D. Rudhardt, P. Leiderer, R. Roth, and S. Dietrich, Phys. Rev. Lett. **83**, 3960 (1999).

[9] L. Helden, R. Roth, G. H. Koenderink, P. Leiderer, and C. Bechinger, Phys. Rev. Lett. **90**, 048301 (2003).

[10] M. Kinoshita, Chem. Phys. Lett. **387**, 47 (2004).

[11] J. R. Henderson, Mol. Phys. **50**, 741 (1983).

[12] M. Kinoshita, J. Chem. Phys. **116**, 3493 (2002).

[13] M. Kinoshita, Chem. Eng. Sci. **61**, 2150 (2006).

[14] Y. Mao, M. E. Cates, and H. N. W. Lekkerkerker, Phys. Rev. Lett. **75**, 4548 (1995).

[15] Y. Mao, M. E. Cates, and H. N. W. Lekkerkerker, J. Chem. Phys. **106**, 3721 (1997).

[16] K. Yaman, C. Jeppesen, and C. M. Marques, Europhys. Lett. **42**, 221 (1998).

[17] R. Roth, J. Chem. Phys. **15**, S277 (2003).

[18] S. M. Oversteegen and H. N. W. Lekkerkerker, Phys. Rev. E **68**, 021404 (2003).

[19] L. Harnau and S. Dietrich, Phys. Rev. E **69**, 051501 (2004).

[20] L. Harnau and S. Dietrich, in *Soft Matter*, edited by G. Gompper and M. Schick (Wiley, Berlin, 2006), Vol. 3.

[21] P. van der Schoot, J. Chem. Phys. **112**, 9132 (2000).

[22] P. van der Schoot, J. Chem. Phys. **113**, 3931 (2000).

[23] R. Roth, R. van Roij, D. Andrienko, K. R. Mecke, and S. Dietrich, Phys. Rev. Lett. **89**, 088301 (2002).

[24] W. Li and H. R. Ma, Eur. Phys. J. E **16**, 225 (2005).

[25] P.-M. König, P. Bryk, K. Mecke, and R. Roth, Europhys. Lett. **69**, 832 (2005).

[26] Y. Rosenfeld, Phys. Rev. Lett. **63**, 980 (1989).

[27] P.-M. König, R. Roth, and K. R. Mecke, Phys. Rev. Lett. **93**, 160601 (2004).

[28] Y. Rosenfeld, Phys. Rev. E **50**, R3318 (1994).

[29] Y. Rosenfeld, Mol. Phys. **86**, 637 (1995).

[30] R. Roth, R. Evans, A. Lang, and G. Kahl, J. Phys.: Condens. Matter **14**, 12063 (2002).

[31] Y.-X. Yu and J. Wu, J. Chem. Phys. **117**, 10156 (2002).